In-line monitoring of compaction properties on a rotary tablet press during tablet manufacturing of hot-melt extruded amorphous solid dispersions.

W. Grymonpré[a], G. Verstraete[a], P.J. Van Bockstal[b], J. Van Renterghem[b], P. Rombouts[c], T. De Beer[b], J.P. Remon[a], C. Vervaet[a,*]

[a] Laboratory of Pharmaceutical Technology, Ghent University, Ghent, Belgium
[b] Laboratory of Pharmaceutical Process Analytical Technology, Ghent University, Ghent, Belgium
[c] Department of Electronics and Information Systems (ELIS), Ghent University, Ghent, Belgium

[*]Corresponding author:

C. Vervaet

Ghent University, Laboratory of Pharmaceutical Technology

Ottergemsesteenweg 460

9000 Ghent (Belgium)

Tel.: +32 9 264 80 54

Fax: +32 9 222 82 36

E-mail address: Chris.Vervaet@UGent.be

Abstract

As the number of applications for polymers in pharmaceutical development is increasing, there is need for fundamental understanding on how such compounds behave during tableting. This research is focussed on the tableting behaviour of amorphous polymers, their solid dispersions and the impact of hot-melt extrusion on the compaction properties of these materials. Soluplus, Kollidon VA 64 and Eudragit EPO were selected as amorphous polymers since these are widely studied carriers for solid dispersions, while Celecoxib was chosen as BCS class II model drug. Neat polymers and physical mixtures (up to 35% drug load) were processed by hot-melt extrusion (HME), milled and sieved to obtain powders with comparable particle sizes as the neat polymer. A novel approach was used for in-line analysis of the compaction properties on a rotary tablet press (Modul P, GEA) using complementary sensors and software (CDAAS, GEA). By combining 'in-die' and 'out-of-die' techniques, it was possible to investigate in a comprehensive way the impact of HME on the tableting behaviour of amorphous polymers and their formulations. The formation of stable glassy solutions altered the formulations towards more fragmentary behaviour under compression which was beneficial for the tabletability. Principal component analysis (PCA) was applied to summarize the behaviour during compaction of the formulations, enabling the selection of Soluplus and Kollidon VA 64 as the most favourable polymers for compaction of glassy solutions.

Keywords: amorphous polymers, hot-melt extrusion, powder compaction, in-line monitoring, rotary tablet press, multivariate data analysis.

1. INTRODUCTION

The interest in biocompatible polymers as substantial components of pharmaceutical formulations is currently growing since they carry a broad spectrum of applications (e.g. pharmaceutical binders, diluents, disintegrants, film coating, release controlling agents and precipitation inhibitors) and can be modified for specific usage (Claeys et al., 2014; Fonteyne et al., 2014; Kadajji and Betageri, 2011; Pillay et al., 2013; Warren et al., 2013; Yang et al., 2010). Furthermore, polymers have been successfully used as stabilizing carriers in solid dispersion manufacturing, a drug formulation that has received a lot of attention in the past few years. The main purpose of formulating a drug as solid dispersion is to ameliorate the bioavailability, since new drug molecules are often poorly water-soluble. Altering the physical state of the active pharmaceutical ingredient (API) by processing it within a polymeric carrier (i.e. solid dispersion) proved to be a viable technique to overcome solubility-related problems (Janssens and Van den Mooter, 2009; Leuner and Dressman, 2000; Vo et al., 2013).

Hot-melt extrusion (HME) is an efficient, continuous process for the manufacturing of solid dispersions as the polymer and API are simultaneously fed into a heated barrel with screws. The combination of heat, mixing, shear and transport finally results in a homogeneous melt in which the drug is preferably molecularly dispersed in the polymer matrix (Sarode et al., 2013; Shah et al., 2013). In respect to dissolution properties, amorphous (glassy) solutions are preferred as they represent the most energetic solid state of a material and therefore amorphous polymers are often used as carrier in solid dispersions (Van Den Mooter, 2012). Downstream processing of the strand-like extrudates by milling and tableting is still one of the preferred techniques to process hot-melt extruded formulations into their final dosage forms (Treffer et al., 2013).

Although there have been many studies on HME and amorphous solid dispersions, there is still limited knowledge on how processing techniques might influence the downstream processing such as the tableting behaviour of pharmaceutical polymers and their formulations (Agrawal et al., 2013; Boersen et al., 2013; Iyer et al., 2013). However, this is a fundamental aspect since it acquires crucial knowledge indispensable for further formulation development. In a previous article (Grymonpré et al., 2016) we illustrated via ‘out-of-die’ methods that HME

altered the mechanical properties of polyvinyl alcohol (PVA, a semi-crystalline polymer), mostly since the physical state of the polymer itself was changed during HME. As amorphous polymers were used in current study, this phenomenon could not occur and evaluating these polymers is therefore beneficial for fundamental investigation of the impact of HME on polymers.

Traditionally, compaction simulators which are designed to simulate the compaction process in a rotary tablet press are used for characterizing 'in-die' compaction properties of pharmaceutical materials (Michaut et al., 2010). Although these devices are versatile and allow in-depth analysis of compaction mechanisms, complex simulations are often necessary for understanding the behaviour in a specific rotary tablet press. Therefore, an experimental approach was developed to monitor and analyse 'in-die' compaction properties of amorphous polymers and their solid dispersions on a rotary tablet press. **It is intended with this research study to validate the feasibility of performing in-line measurements during the tableting process. The relationships in the compaction data were highlighted using PCA in order to establish a formulation development platform of HME processed materials for tableting purpose.**

2. MATERIALS AND METHODS

2.1. Materials

Three commonly used amorphous polymers were selected for this study. Soluplus (SOL) and Kollidon VA 64 (VA 64) were a gift from BASF (Ludwigshafen, Germany) while Eudragit EPO (EPO) was donated by Evonik (Darmstadt, Germany). Celecoxib (CEL, Utag, Amsterdam, The Netherlands), a BCS class II drug, was used as model drug.

2.2. Characterization

2.2.1. Thermal analysis

Thermogravimetric analysis (TGA 2950, TA instruments, Leatherhead, UK) was conducted on all polymers and CEL to investigate the thermal stability. Samples (± 15 mg) were heated up to 600 °C after equilibration at 25 °C using a heating rate of 10 °C/min.

All materials were analysed via modulated differential scanning calorimetry (MDSC) (Q2000, TA Instruments, Leatherhead, UK) to detect glass transition temperatures (T_g) and melting points (T_m) using a heating rate of 2 °C/min and a modulation of 0.318 °C/min over 3 cycles (heat/cool/heat) from -20 °C to 200 °C. The (M)DSC cell was purged with dry nitrogen at a flow rate of 50 ml/min. All results were analysed in triplicate using the TA instruments Universal Analysis 2000 software. Additional MDSC-measurements (2 cycles) were performed both after HME and milling in order to verify the solid state properties of all formulations after each processing step. A one-way analysis of variance (ANOVA) was performed with SPSS Statistics 23 (IBM, New York, United States) to detect significant differences in T_g after extrusion or milling. A Shapiro-Wilk test was performed to verify normality and the homogeneity of variances was tested by Levene statistics. Tukey analysis was used to determine differences in T_g and T_m between non-processing, extrusion or milling.

2.2.2. *X-ray diffraction*

X-ray Diffraction patterns (XRD) were recorded to investigate the crystallinity of the formulations before and after HME/milling using a D5000 CU Kα diffractor (λ=0.154 nm) (Siemens, Karlsruhe, Germany) with a voltage of 40 V in the angular range of 10 ° < 2θ < 20 ° using a step scan mode (step width = 0.02 °, counting time = 1 s/step).

2.2.3. *Fourier-transform infrared spectrometry*

Attenuated total reflection Fourier-transform infrared (ATR FT-IR) spectrometry (Thermo Fisher Scientific, Nicolet iS5, Massachusetts, USA) was applied to examine interactions between polymers and API. Spectra (n=3) were collected in the 4000-550 cm^{-1} range with a resolution of 4 cm^{-1} and averaged over 64 scans for all formulations (neat polymers, polymer-API physical mixtures and milled solid dispersions). SIMCA 13.0.3 software (Umetrics, Umeå, Sweden) was used for data analysis and standard normal variate (SNV) pre-processing of the FT-IR spectra.

2.2.4. *Particle size distribution*

Particle size distribution (PSD) of the powders was recorded (n=3) by laser diffraction (Mastersizer-S long bench, Malvern Instruments, Malvern, UK) via a dry dispersion method in volumetrical distribution mode using a 300 RF lens combined with a dry powder feeder at a feeding rate of 3.0 G and a jet pressure of 2.0 bar (Malvern Instruments, Malvern, UK).

2.2.5. *Helium pycnometry*

True density of all powders was measured (n=3) using helium pycnometry (AccuPyc 1330, Micromeritics, Norcross, USA) at an equilibration rate of 0.0050 psig/min with the number of purges set to 10. Calibration was performed between the formulations.

2.2.6. Moisture content

Immediately before tabletting, loss on drying (LOD) was performed (n=3) on all formulations to determine residual moisture content using a Mettler LP16 moisture analyser, including an infrared dryer and a Mettler PM460 balance (Mettler-Toledo, Zaventem, Belgium). Approximately 1 g of sample was dried at 105 °C until the rate of change was less than 0.1% w/w for 30 s.

2.2.7. Specific surface area

Specific surface area (SSA) of the powders was measured using krypton gas adsorption (ASAP 2420, Micromeritics, Norcross, USA) with multipoint BET (Brunnauer, Emmett, and Teller) calculations per ISO 9277. All samples were outgassed under vacuum at 25 °C for 960 minutes to remove any gases and vapours that may have adsorbed on the surface. The relative pressures (P/P_0) during the measurements ranged from 0.05 to 0.25 (11 datapoints) at a temperature of -196 °C and an equilibration interval of 10s.

2.2.8. Powder flowability

The flow rate of all formulations was determined using a flowability testing device (FlowPro, IPAT, Finland) which consists of a frame, sample holder (5.96 ml) with orifice (3.0 mm) and an analytical scale. Vertical oscillations of the sample holder break the cohesive forces in the powder bed and allow the powder to flow through the orifice. The mass discharged from the sample holder is measured over time in order to calculate the flow rate (mg/s) (Sandler et al., 2010). 5% of the mass flow function at the beginning and at the end was not taken into account to minimize the non-linearity of the mass flow (Seppälä et al., 2010). All samples were measured in triplicate.

2.3. Screening drug load capacity

Physical mixtures of each polymer and CEL were made with mortar and pestle, and afterwards extruded on a co-rotating twin-screw extruder (Haake MiniLab II Micro Compounder, Thermo Electron, Karlsruhe, Germany) at a screw speed of 70 rpm and different processing temperatures (130 °C for EPO-mixtures; 150 °C for SOL-mixtures and 160 °C for VA 64-mixtures). Modulated differential scanning calorimetry (MDSC) was used for solid state characterization of the resulting extrudates and detecting the maximal solubilising capacity of each polymer for the drug.

2.4. Rheological screening for hot-melt extrusion

Rheological properties of all polymers and their physical mixtures (35% CEL, w/w) were determined with a Thermo Scientific HAAKE MARS III (Modular Advanced Rheometer System, Thermo Fisher Scientific, Karlsruhe, Germany) in order to predict the extrudable temperature range for each formulation. A parallel plate (d = 20 mm) geometrical set-up was used and all measurements were done in a control deformation auto strain mode. At first, an amplitude sweep was performed on all samples to determine the linear viscoelastic region. Afterwards, the samples were loaded at 90 °C and equilibrated for 5 min to perform a temperature sweep. All samples were gradually heated at 2 °C/min with an angular frequency of 1 Hz and a strain rate of 1% (for SOL and VA 64 - mixtures) or 5% (for EPO mixtures) in order to determine the temperature range for which the complex viscosity (η^*) is between 1000 and 10000 Pa s (Gupta et al., 2015; Verstraete et al., 2016).

2.5. Hot-melt extrusion

Both neat polymers and their physical mixtures (containing 35% CEL, w/w) were extruded using a co-rotating, fully intermeshing twin-screw extruder (Prism Eurolab 16, Thermo Fisher, Germany) equipped with two co-rotating twin-screws with 3 mixing zones, a cylindrical

die of 3 mm and a DD flexwall® 18 feeder (Brabender Technology, Germany), which was set in its gravimetric feeding mode. HME was conducted at a screw-speed of 75 rpm and barrel temperatures depending on the rheological screening (Table 1). The resulting extrudates were milled after cooling using a knife mill (Moulinex AR110510, France) and sieved towards equal particle sizes as the neat non-processed polymers.

2.6. Tableting

For each polymer, 3 formulations (neat polymer, neat polymer extrudates and extrudates of polymer-CEL (35%)) were compressed to tablets on a rotary tablet press (MODUL™ P, GEA Pharma Systems, Courtoy™, Halle, Belgium) equipped with cylindrical flat-faced Euro B punches of 10 mm diameter and an overfill cam of 16 mm. Tablets (270 ± 10 mg) were compressed on 6 different main compaction pressures: 65, 130, 190, 255, 380 and 510 MPa without the use of a pre-compression step at a turret speed of 5 rpm. All tablets were analysed for 'out-of-die' properties (tablet strength, dimensions and mass) immediately after ejection. Punch deformation at each compaction pressure was calculated and corrected for during this study. Tableting and tablet characterization was performed in a climatic chamber, for which the temperature and relative humidity were recorded at 24.7 (± 0.6) °C and 36.4 (± 1.5)% respectively.

In-die measurements of the compaction properties was performed by linear variable displacement transducers (LVDT) incorporated inside the turret and clamped onto one pair of punches enabling the monitoring of punch stroke movements during a compression cycle (GEA Pharma Systems, Halle, Belgium). Calibration was done previous to each formulation, by interpolating the output voltage of the sensor to physical values during static measurements. A wireless transmission system continuously transmitted the data from these sensors to a data acquisition and analysis system (CDAAS, GEA Pharma Systems, Halle, Belgium).

2.7. Compaction process evaluation

2.7.1. 'Out-of-die' measurements

Tablet diametrical tensile strength was calculated according to following equation (Fell, J.T.; Newton, 1968):

$$Tablet\ Tensile\ Strength\ (\sigma_t) = \frac{2P}{\pi Dt} \quad (1)$$

where *P*, *D* and *t* denotes tablet diametral breaking force (N), tablet diameter (mm) and tablet thickness (mm), respectively, which are determined using a hardness tester (Sotax HT10, Basel, Switzerland).

In order to determine the porosity of the compacts following equation is used:

$$Tablet\ Porosity = 1 - \frac{\rho_{app}}{\rho_{true}} \quad (2)$$

where ρ_{app} and ρ_{true} denote the apparent and true density (g/ml), respectively. The latter was measured using helium pycnometry (AccuPyc 1330, Micrometrics, Norcross, USA), while the apparent density was calculated by dividing the tablet mass by the volume of the tablet.

Tabletability and compressibility profiles of each formulation were analysed by plotting tablet tensile strength and porosity, respectively, in function of the main compaction pressure. Compactibility of the formulations was assessed by plotting log tensile strength in function of tablet porosity, a relationship that was described by (Ryshkewitch, 1953):

$$\sigma_t = \sigma_0\, e^{-bP} \quad (3)$$

where σ_t and σ_0 denotes the tablet tensile strength (MPa) and limiting tablet tensile strength at zero porosity (MPa), respectively, *b* is an empirical constant and *P* denotes the tablet porosity.

'Out-of-die' axial recovery (AR) of the compacts was calculated based on following equation (Armstrong and Haines-Nutt, 1972):

$$AR\ (\%) = \left(\frac{Ta - Tid}{Tid}\right) x100 \quad (4)$$

for which T_{id} represents the minimal tablet thickness (mm) under maximal compression force 'in-die' and T_a is the tablet thickness (mm) measured immediately after ejection and after 7

days of storage in hermetic sealed aluminium bags (AR_7) by use of a validated micrometre screw.

2.7.2. 'In-die' measurements

Measuring the punch stroke movement during compression on the instrumented rotary tablet press enabled plotting of the compression cycles, taking into account the compaction force and the punch separation (i.e. force-displacement curves, **Fig. 1**). During a compression cycle on a rotary tablet press, upper and lower punch are moving towards each other inducing consolidation of the powder bed. In a first phase (A-A'), the powder particles are rearranged and packed without any measurable increase in compression force up to a second phase (A'-B) that is characterised by an augmentation of compression force until a maximal force is reached (B) correlating with minimal separation between upper and lower punch (C, i.e. minimal tablet thickness). During this second phase, particle fragmentation, plastic deformation and rearrangement occurs (depending on the material properties), resulting in varying degrees of particle consolidation. The final phase of the compression cycle (B-D) is marked by a progressive release of applied stress where a period of elastic recovery (i.e. dissipation of stored elastic energy) by the compact can re-enlarge the distance between upper and lower punch (D).

Energy consumption or dissipation (J/g) at each phase can be calculated from the area under the curve:

$$E = \int F \, dh \tag{5}$$

where *F* denotes the compression force (kN) and *h* the punch separation (mm). All energies are normalised by taking the compact mass into account to allow comparison between the different formulations.

The integral calculus from A' to C (**Fig. 1**) corresponds to the specific total energy (A'BD) involved in compression excluding packing and frictions (A-A'), used for fragmentation and deformation which induce interparticulate bonding. The specific expansion energy (i.e.

energy lost by instantaneous (in-die) elastic recovery of the compact, BCD) is calculated by integration from C to D (**Fig. 1**). The difference between total energy and expansion energy defines the (specific) net energy during compaction (A'BD) (Busignies et al., 2004; Michaut et al., 2010; Pontier et al., 2002; Rodriguez and Chulia, 2005; Vachon and Chulia, 1999).

The resulting energies are used for calculation of two specific compaction properties:

- A plasticity factor (PF) which represents the energy of compaction used for plastic deformation and fragmentation:

$$PF\ (\%) = \frac{net\ energy}{total\ energy}\ x\ 100 \quad (6)$$

- 'In-die' axial recovery (IAR) which represents the elasticity of a material:

$$IAR\ (\%) = \frac{Td-Tc}{Tc}\ x\ 100 \quad (7)$$

where T_d and T_c represents the punch separation after decompression (point D at **Fig. 1**) and the minimal punch separation during compression (point C at **Fig. 1**), respectively.

All calculations for in-line measuring of the compaction properties were done using the CDAAS software (GEA Pharma Systems, Halle, Belgium) on at least 3 compacts for each formulation.

Using the 'in-die' data of the CDAAS system, Heckel analysis was performed on all formulations using the data at a compaction pressure of approximately 65 MPa. The theory of Shapiro-Konopicky-Heckel is based on following equation (Heckel, 1961):

$$ln\ \frac{1}{E} = KP + A \quad (8)$$

where E is the porosity of the powder bed at a compaction pressure P, K is the slope of the linear part of the plot (with the best R^2 fit) and A is the Y intercept with the linear part of the plot. The mean Heckel yield pressures (P_y) are given by the reciprocal values K, while the intercept of both the linear part of the plot (A) and the non-linear part (I) are used to calculate D_a, D_I.

$$D_{a\,(I)} = 1\text{-}\,e^{-A\,(I)} \quad (9)$$

The difference between D_a and D_I denotes D_b, which describes the reduction in volume due to rearrangement of the particles since A is said to reflect low pressure densification by interparticulate motion (Tarlier et al., 2015).

$$D_b = D_a - D_I \tag{10}$$

2.8. Multivariate data analysis

Principal component analysis (PCA) was executed on the relevant compaction data in order to classify the different materials according to their compaction behaviour by using the multivariate data analysing software SIMCA 13.0.3 (Umetrics, Umeå, Sweden). PCA is a multivariate projection method which extracts and displays the variation in the data set (Pieters et al., 2013). Highly correlated original variables, e.g. relevant compaction and mechanical properties of the formulations, are transformed into a new system of latent variables called principal components (PCs) which are sequentially acquired by an orthogonal, bilinear decomposition of the data matrix. PCs are composed of a scores and a loading vector. The loading vector provides qualitative information about which properties in the original observations are captured by the corresponding component, while the scores (i.e. the associated weighted averages of the original variables) provide quantitative information on how the different materials behave under compaction. The data were pre-processed by unit variate scaling and centered in order to balance the weight of each variable.

3. RESULTS AND DISCUSSION

3.1. Material characterization & extrusion screening

TGA indicated that all components of the formulations were thermally stable at the temperatures used in HME as degradation of the most sensitive component (CEL) occurred from 242 °C (**Table 1**) and extrusion temperatures of the formulations containing CEL did not exceed 150 °C. MDSC measurements confirmed that all polymers were amorphous, while a melting endotherm was detected for CEL around 162 °C. Rheological properties of the formulations were investigated in order to predict the required HME temperatures, as this approach was more effective compared to predictions based on MDSC data since the samples are additionally subjected to shear stresses during the rheology measurements (Gupta, 2014). Gupta et al. stated that the temperature range where the melt viscosity of a polymer ranges between 1000 and 10000 Pa s is the most suitable region for melt extrusion (Gupta et al., 2015). This region was determined by linking observed torque values during HME with the complex viscosity of SOL-formulations. Using temperature sweeps experiments (**Fig. 2**), the extrudable regions were established for the amorphous polymers used in this study and based on these data the barrel temperatures for the HME experiments were determined (**Table 1**).

Maximal solubilising capacity of each polymer for CEL was screened by MDSC-measurements on the extrudates. Up to 35% of CEL could be dispersed in all polymer carriers while obtaining stable glassy solutions, since no melting endotherm appeared in the thermograms and only one T_g was present. At higher drug loads CEL melting peaks were detected.

3.2. Solid state characterization

MDSC analysis was used to examine the influence of extrusion and milling on the solid

state physicochemical properties of the intermediate products (**Table 2**). ANOVA showed a significant ($p<0.05$) drop in polymer T_g after HME of the neat polymers, a phenomenon that has been linked to an increase in free volume between the polymer strains due to the shear stress (Pae and Pressure, 1986). This was significant for SOL and EPO, since they have a lower T_g and therefore a less rigid structure compared to VA 64. Milling did not have a significant ($p>0.05$) influence on T_g for all formulations.

Processing the physical mixtures (PM) of all polymers with CEL by HME yielded glassy solutions with a single T_g. However, the presence of only one T_g does not necessarily indicates drug-polymer miscibility since the T_g of CEL and SOL/EPO were close to each other (Van Den Mooter, 2012). Therefore, additional XRD-analysis and FT-IR spectrometry was applied on the formulations in order to distinguish between the solid dispersion type. X-ray diffraction patterns confirmed the absence of crystalline content (typical amorphous halo) in solid dispersions of SOL, VA 64 and EPO (c, e, g respectively in **Fig. 3**) compared to their non-processed physical mixtures (b, d, f respectively in **Fig. 3**).

FT-IR measurements were used to identify possible molecular interactions between drug (CEL) and polymers after HME, which is an indication for good stabilizing properties of the carriers. Relevant parts of the FT-IR spectra were the stretching vibrations in the area from 3500 till 2800 cm^{-1}, as highlighted in **Fig. 4** for SOL-formulations. A specific fingerprint of CEL was detected in the physical mixtures with abundant bands at 3333, 3227 and 3062 cm^{-1} (**Fig. 4**). The sharp doublet at 3333 cm^{-1} and 3227 cm^{-1} is attributed to the N-H stretching vibration of the $-SO_2NH_2$ group of CEL. This doublet was clearly diminished and broadened after HME, suggesting that the sulphonamide group of CEL acted as H-donor and engaged in interactions with –C=O carbonyl groups (H-acceptors) of the polymer (Fouad et al., 2011; Gupta et al., 2005). Similar spectra were obtained for the solid dispersions with VA 64 and EPO (data not shown), which were in line with earlier findings linking this spectra to the formation of an amorphous drug form and possible molecular interactions between CEL and the carriers (Albers et al., 2009), favouring stability of the formulation. By combining the data from MDSC, XRD and FT-IR measurements, it was concluded that HME resulted in the formation of glassy

solutions.

Accelerated stability tests were conducted on the glassy solutions under stress conditions (40 °C and 75% relative humidity) as described by the ICH Q1A (R2) guidelines. Glassy solutions of all formulations containing 35% of CEL (milled extrudates) were stable for at least 6 months under these conditions since MDSC revealed no reappearance of the T_m specific for CEL. These results emphasized that the selected amorphous polymers were suitable carriers for solid dispersions with CEL as they had sufficient stabilizing properties.

3.3. Powder characterization

Before tableting, all powders (neat polymers and milled extrudates) were investigated on their true density, moisture content, particle size distribution, specific surface area and flowability since these could impact the tableting behaviour of the formulations (**Table 3**). LOD measurements revealed no significant differences in moisture content between the neat polymers and the processed formulations (i.e. milled extrudates), which was beneficial for this study since these results excluded the moisture content as a confounding factor during analysis of the tableting behaviour of the formulations. During the study, it was essential to limit differences in PSD in order to be able to compare similar formulations on their tableting behaviour before and after HME processing. Therefore, the milled extrudates were extensively sieved to obtain a PSD similar to the neat polymer.

When comparing specific surface areas of the samples, most variation was noticed between the polymer types which could be explained by differences in PSD between formulations of SOL, VA 64 and EPO. However, particle size and surface area are not completely interchangeable since this correlation is also dependent on the shape of the particles.

Flowability of the powders was mainly dependent on the mean PSD (**Table 3**). With respect to flowability, the polymers are ranked in the following decreasing order: SOL, VA 64 and EPO. Impact of the processing steps on the flowability of formulations within one polymer

was small, suggesting that the flowability of the formulations mainly depended on the initial flow properties of the neat polymer.

3.4. Tablet properties

3.4.1. 'Out-of-die' measurements

The impact of HME on the tabletability of the formulations is shown in **Fig. 5**, which describes the ability of a material to form compacts with a certain tensile strength in function of the compaction pressure. Briefly, tablet tensile strength increased when higher pressures were exerted on the powder bed until a certain point where, material-depending, the stored elastic energy of the materials caused a level-off (i.e. plateau phase) in the profile (Sun, 2011). When analysing tabletability plots, both the relative positioning of the curves (i.e. maximal tabletability) and more importantly the shape of the curves (i.e. inflection point for level-off) should receive attention, since the latter indicates whether changes in mechanical properties have occurred during HME (Grymonpré et al., 2016). The largest influence of HME on the tabletability profiles was noticed for formulations containing SOL and EPO (**Fig. 5**). In general, tablets with higher tensile strength were obtained when tableting glassy solutions (polymer-CEL) compared to tablets of the neat polymer or their extrudates, except for glassy solutions of VA 64 which yielded tablets with low tensile strength at low forces. Additionally, differences were obtained in the curve-shape of the glassy solutions as maximum tabletability was reached at higher compaction pressures, indicating altered mechanical properties for this formulation, while HME had no impact on this parameter for the neat polymer (i.e. similar curve-shape for the neat polymer and their extrudates). Tablets of SOL-extrudates have slightly lower tensile strengths compared to tablets of the non-processed polymer although the shape of the curve remains the same. This could be due to small changes in the bonding area (reflected by the compressibility) and/or changes in the bonding strength per unit bonding area (reflected by the compactibility).

Compressibility plots describe the ability of a material to reduce its volume as result of an applied pressure and can be used for comparing the tendency of a formulation to create sufficient interparticulate bonding area (i.e. lower porosity) under pressure (Sun and Grant, 2001). When analysing the compressibility profiles (**Fig. 6**), slightly lower porosities were obtained for tablets of EPO-extrudates, indicating higher interparticulate bonding areas which could explain the higher tabletability for this formulation in combination with the higher specific surface areas measured for this formulation (**Table 3**). No significant differences in compressibility were detected for formulations with SOL and VA 64. Therefore, the lower tabletability of SOL-extrudates could not be attributed to lower interparticulate bonding areas for this formulation.

Tablet tensile strength decreases exponentially with increasing porosity as formulated in the Ryshkewitch equation (Ryshkewitch, 1953) and is described by the compactibility (**Fig. 7**) as a measure for the bonding strength per unit bonding area. By analysing compactibility, the origin of the differences in tablet tensile strength for SOL-formulation was detected, since extrudates of SOL showed lower interparticulate bonding strength at a specific porosity compared to the neat polymer and the glassy solutions. The compactibility plots for VA 64 and EPO were in line with the tabletability plots, a better compactibility for glassy solutions at lower porosities (i.e. higher compaction pressures).

Simultaneously investigating compressibility and compactibility of the formulations enabled to explain the differences observed in the relative positioning of the tabletability plots. In general, the higher tablet tensile strengths observed for glassy solutions formulated with all polymers were due to higher interparticulate bonding strengths per unit bonding area (i.e. compactibility), while no changes were detected in the interparticulate bonding areas between formulations. However, these ‘out-of-die’ techniques could not fully explain the altered shape of the tabletability curves, which are indicative of a modified compaction behaviour, and did not resulted in a comprehensive understanding of the formation of higher interparticulate bonding strengths. Therefore, there was need for analysing the compaction properties of these formulations to understand the mechanisms which modified the mechanical properties such

as tablet tensile strength. These compaction properties focus more on how a material uses the energy provided during the different stages of a compression cycle, by analysing energy plots (i.e. force-displacement curves) of the formulations (Busignies et al., 2004).

3.4.2. 'In-die' measurements

During this study an experimental approach was used to measure the 'in-die' compaction properties of formulations containing amorphous polymers immediately on a fully instrumented rotary tablet press. **Fig. 8** displays the plasticity factor, which represents the energy used during compaction for plastic deformation and fragmentation, in function of the compaction pressure exerted on the powder bed.

Although two completely independent data sets were used, there was a remarkably good correlation between these plasticity factor profiles and the tabletability plots of the same formulations. For SOL-formulations, the plasticity factor of the glassy solutions started to deviate from the neat and extruded polymer at 190 MPa (**Fig. 8,** left), similar to the compaction pressure at which differences in tablet tensile strength started to occur between the SOL formulations (**Fig. 5,** left). Similar correlations between the plasticity factor profiles and tabletability plots were observed for VA 64 and EPO formulations. At higher compaction pressures, glassy solutions of SOL and EPO underwent more plastic deformation which could explain the higher compactibility and tabletability of this formulations, while glassy solutions of VA 64 initially underwent less plastic deformation at lower compaction pressures which was correlated with the tabletability plots of this polymer. No differences in plasticity factor were detected between tableting the neat polymers and their extrudates, indicating that HME did not alter the volume reduction mechanisms of the amorphous polymers when no API is included.

Fig. 9 shows the measured in-die elastic recovery (IER), which represents the elasticity of a material, plotted against the compaction pressure. If a material has more elastic properties it can release the stored elastic energy from compression during the decompression phase, thereby causing disruption of some previously formed interparticulate bondings, resulting in a

higher IER and often lower tablet tensile strength (i.e. plateau phase in tabletability). More elastic recovery during decompression was recorded at higher compaction pressures since more energy is provided to be stored by the particles as elastic energy. No differences in IER were noticed between SOL and VA 64-containing formulations, while a significantly lower IER was obtained for glassy solutions of EPO compared to the neat polymer and its extrudates. This could contribute to the higher tabletability of EPO-glassy solutions since less interparticulate bondings formed during compaction are disrupted during decompression.

Analysis of the Heckel plots (**Fig. 10**) allowed to calculate several 'in-die' properties, summarized in Table 4. For each polymer type, a significantly higher P_y value was noticed for the glassy solutions, combined with higher D_b values. The Heckel yield pressure is often used as indication of particle plasticity (Klevan et al., 2010), while D_b values represent the particle rearrangement in the low pressure region whereby higher D_b values are indicative of materials with higher fragmentary nature (Tarlier et al., 2015). These values indicated that the glassy solutions underwent more volume reduction upon rearrangement compared to the other formulations because of their higher fragmentary behaviour (i.e. higher D_b and P_y values). As fragmentation resulted in smaller particle sizes (in-die), tensile strength of such formulations will be higher as seen in the tabletability plots (**Fig. 5**). As explained by Nordström et al., the hardness of the particles can be estimated based on P_y values (Nordström et al., 2012) whereby the particles of the formulations included in this study were categorized as soft (i.e. 40 MPa < P_y < 80 MPa) or moderately hard (i.e. 80 MPa < P_y < 200 MPa).

3.4.3. Tablet axial recovery over time

Knowledge on the elastic behaviour of tableting formulations is essential to formulate compacts with adequate tensile strength and for the compaction process itself (e.g. capping issues), but it also has its value in downstream processing of tablets. The coating of tablets can be essential for various reasons (e.g. taste masking), but it is a major challenge for industry to step down from the batch-wise coating processes towards a continuous (coating) process

after tableting. Limited knowledge is provided on the time dependency of elastic recovery for tablets made of polymer formulations although this is critical information in relation to the (continuous) coating process. Therefore, in addition to the 'in-die' elastic recovery of the tablets (as described above), elastic recovery of the tablets was monitored 'out-of-die' immediately after ejection and after storage over 7 days for monitoring the entire recovery process of tablets formulated with these amorphous polymers (**Fig. 11**). Radial dimension changes were negligible compared to the axial changes, as expected since pressure is applied in axial direction during compression (Haware et al., 2010; Picker, 2001).

A similar linear relationship between elastic (axial) recovery and compaction pressure was noticed, but the values recorded 'out-of-die' were higher compared to those measured 'in-die'. This indicated that a substantial part of the total tablet axial recovery took place after ejection from the die. Tablets of glassy solutions underwent less 'out-of-die' axial recovery compared to the formulations without API, which is beneficial for the tableting process (i.e. reducing the risk of capping), while the differences between the neat polymers and HME polymers were marginal, confirming the 'in-die' data where HME had no impact on the elastic properties of the neat polymers. No significant changes in axial tablet dimensions were recorded after 7 days storage of SOL and VA 64 tablets, suggesting a short timeframe for elastic recovery which makes these polymers beneficial for usage in (continuous) coating-processes compared to EPO tablets.

3.5. Multivariate data analysis

In order to summarize the behaviour under compaction of all formulations in a comprehensive way, a multivariate approach was used where the different compaction and mechanical properties were combined in order to classify the formulations according to the contributions of individual properties. PCA has previously been used to interpret the mechanical behaviour of pharmaceutical materials (Roopwani et al., 2013). The two principal components in the current PCA accounted for 94.1% of the total variance in the dataset with

the first and the second principal component (PC_1 and PC_2) comprising 68.8% and 25.3%, respectively.

Analysis of the bi-plot (**Fig. 12**) for both principal components (PC_1 and PC_2) enabled to cluster formulations with similar properties. In the direction of PC_1, a cluster of the EPO-formulations (left of the origin) and a cluster of SOL and VA 64 formulations (right of the origin) was observed. The loadings indicated that PC_1 differentiated the plastic deformation potential of a material (represented by the plasticity factor), while it was anti-correlated with the elastic recovery of materials (represented by IER). Materials with a high tendency for elastic recovery (high IER) are located left (i.e. EPO-formulations), while the materials which deform more plastically (high plasticity factor) are located right of the origin. In addition, PC_1 captured the flow-properties of materials as good flowing materials were positioned to the right. The scores also indicated that the glassy solutions of all polymer types were clustered at higher PC2 values. PC_2 gave information about the fragmentation behaviour of the material (i.e. high D_b and P_y values) as the glassy solutions of the polymers were identified by high PC2. Inevitable, these materials will show higher tensile strength at zero porosity (σ_0) which is also shown by the loadings in the bi-plot.

The use of PCA enabled the selection of amorphous polymers which have the highest potential as carrier for glassy solutions with CEL in respect of tableting. This was done by making an imaginary arrow (**Fig. 12**) from the bottom left side (least favourable) of the bi-plot towards the upper right side (most favourable) and projecting the scores orthogonal on this line. In this case, SOL and VA 64 glassy solutions had the best compaction and flow properties making the selection of these amorphous polymers beneficial compared to EPO.

4. CONCLUSIONS

Monitoring the punch movement using the described instrumentation and CDAAS-software was an effective tool for in-line measurement of compaction properties on a rotary tablet press. These compaction properties provided better insight in the compression mechanisms which enable the formation of strong compacts. By combining both ‘in-die’ and ‘out-of-die’ techniques it was possible to investigate in a comprehensive way the impact of HME on the tableting behaviour of amorphous polymers and their formulations. While HME had only a limited influence on the compaction properties of the amorphous polymers when no drug was included, HME changed the compaction properties of glassy solutions towards a

more fragmentary behaviour, independent of the type of amorphous polymer. **The application of PCA on the compaction data empowered the selection of SOL and VA 64 from the polymer platform as favourable amorphous polymers over EPO. This research paper offered a straightforward approach for the establishment of a formulation development platform from which researchers could select the adequate polymer for both HME and tableting purpose.**

Acknowledgements

The authors would like to thank Nazilya Nabirova and Camille Vanhoutte for their experimental help and GEA Pharma Systems for providing the complementary tooling for measuring punch displacement on the rotary tablet press.

5. LITERATURE

Agrawal, A.M., Dudhedia, M.S., Patel, A.D., Raikes, M.S., 2013. Characterization and performance assessment of solid dispersions prepared by hot melt extrusion and spray drying process. Int. J. Pharm. 457, 71–81.

Albers, J., Alles, R., Matthée, K., Knop, K., Schulze, J., Kleinebudde, P., 2009. Mechanism of drug release from polymethacrylate-based extrudates and milled strands prepared by hot-melt extrusion. Eur. J. Pharm. Biopharm. 71, 387–394.

Armstrong, N.A., Haines-Nutt, R.F., 1972. Elastic recovery and surface area changes in compacted powder systems. J. Pharm. Pharmacol. 24, 135-136.

Boersen, N., Lee, T.W-Y., Shen, X.G., Hui, H-W., 2013. A preliminary assessment of the impact of hot-melt extrusion on the physico-mechanical properties of a tablet. Drug Dev. Ind. Pharm. 9045, 1–9.

Busignies, V., Tchoreloff, P., Leclerc, B., Besnard, M., Couarraze, G., 2004. Compaction of crystallographic forms of pharmaceutical granular lactoses. I. Compressibility. Eur. J. Pharm. Biopharm. 58, 569–576.

Claeys, B., De Bruyn, S., Hansen, L., De Beer, T., Remon, J.P., Vervaet, C., 2014. Release characteristics of polyurethane tablets containing dicarboxylic acids as release modifi ers – a case study with diprophylline. Int. J. Pharm. 477, 244–250.

Fell, J.T.; Newton, J.M., 1968. The tensile strength of lactose tablets. J.Pharm.Pharmacol. 20,

658–675.
Fonteyne, M., Luke, A., Vercruysse, J., Vervaet, C., Remon, J.P., Strachan, C., Rades, T., De Beer, T., 2014. Distribution of binder in granules produced by means of twin screw granulation. Int. J. Pharm. 462, 8–10.
Fouad, E.A., El-badry, M., Mahrous, G.M., Alanazi, F.K., Neau, S.H., Alsarra, I.A., 2011. The use of spray-drying to enhance celecoxib solubility. Drug Dev. Ind. Pharm. 37, 1463–1472.
Grymonpré, W., De Jaeghere, W., Peeters, E., Adriaensens, P., Remon, J.P., Vervaet, C., 2016. The impact of hot-melt extrusion on the tableting behaviour of polyvinyl alcohol. Int. J. Pharm. 498, 254–262.
Gupta, P., Thilagavathi, R., Chakraborti, A.K., Bansal, A.K., 2005. Differential molecular interactions between the crystalline and the amorphous phases of celecoxib. J. Pharm. Pharmacol. 57, 1271–1278.
Gupta, S.S., 2014. Application of rheology and phase analysis to melt extrusion: effects of product and process parameters. St. John's University (New York).
Gupta, S.S., Parikh, T., Meena, A.K., Mahajan, N., Vitez, I., Serajuddin, A.T.M., 2015. Effect of carbamazepine on viscoelastic properties and hot melt extrudability of Soluplus. Int. J. Pharm. 478, 232–239.
Haware, R.V., Tho, I., Bauer-Brandl, A., 2010. Evaluation of a rapid approximation method for the elastic recovery of tablets. Powder Technol. 202, 71–77.
Heckel, R.W., 1961. An analysis of powder compaction phenomena. Trans. Met. Soc. AIME 1001–1008.
Iyer, R., Hegde, S., Zhang, Y.E., Dinunzio, J., Singhal, D., Malick, A., Amidon, G., 2013. The impact of hot melt extrusion and spray drying on mechanical properties and tableting indices of materials used in pharmaceutical development. J. Pharm. Sci. 102, 3604–3613.
Janssens, S., Van den Mooter, G., 2009. Review: physical chemistry of solid dispersions. J. Pharm. Pharmacol. 61, 1571–1586.
Kadajji, V.G., Betageri, G. V, 2011. Water Soluble Polymers for Pharmaceutical Applications. Polymers (Basel). 3, 1972–2009.
Klevan, I., Nordström, J., Tho, I., Alderborn, G., 2010. A statistical approach to evaluate the potential use of compression parameters for classification of pharmaceutical powder materials. Eur. J. Pharm. Biopharm. 75, 425–435.
Leuner, C., Dressman, J., 2000. Improving drug solubility for oral delivery using solid dispersions. Eur. J. Pharm. Biopharm. 50, 47–60.
Michaut, F., Busignies, V., Fouquereau, C., Huet De Barochez, B., Leclerc, B., Tchoreloff, P., 2010. Evaluation of a Rotary Tablet Press Simulator as a Tool for the Characterization of Compaction Properties of Pharmaceutical Products. J. Pharm. Sci. 99, 2874–2885.
Nordström, J., Klevan, I., Alderborn, G., 2012. A protocol for the classification of powder compression characteristics. Eur. J. Pharm. Biopharm. 80, 209–216.
Pae, K.D., Pressure, H., 1986. Effect of simple stress on the glass transition of polymers at high pressures. J. Mater. Sci. 21, 2901–2907.
Picker, K.M., 2001. Time Dependence of Elastic Recovery for Characterization of Tableting Materials. Pharm. Dev. Technol. 6, 61–70.
Pieters, S., Vander Heyden, Y., Roger, J.M., DHondt, M., Hansen, L., Palagos, B., De Spiegeleer, B., Remon, J.P., Vervaet, C., De Beer, T., 2013. Raman spectroscopy and multivariate analysis for the rapid discrimination between native-like and non-native states in freeze-dried protein formulations. Eur. J. Pharm. Biopharm. 85, 263–271.
Pillay, V., Seedat, A., Choonara, Y.E., Toit, L.C., Kumar, P., Ndesendo, V.M.K., 2013. A Review of Polymeric Refabrication Techniques to Modify Polymer Properties for Biomedical and Drug Delivery Applications. AAPS PharmSciTech 14, 692–711.
Pontier, C., Champion, E., Viana, M., Chulia, D., Bernache-Assollant, D., 2002. Use of cycles of compression to characterize the behaviour of apatitic phosphate powders. J. Eur. Ceram. Soc. 22, 1205–1216.
Rodriguez, F., Chulia, D., 2005. Powder Functionality Test : A Methodology for Rheological and Mechanical Characterization. Pharm. Dev. Technol. 10, 327–338.

Roopwani, R., Shi, Z., Buckner, I.S., 2013. Application of Principal Component Analysis (PCA) to Evaluating the Deformation Behaviors of Pharmaceutical Powders. J. Pharm. Innov. 8, 121–130.
Ryshkewitch, E., 1953. Compression Strength of Porous Sintered Alumina and Zirconia. J. Am. Ceram. Soc. 36, 65–68.
Sandler, N., Reiche, K., Heinämäki, J., Yliruusi, J., 2010. Effect of Moisture on Powder Flow Properties of Theophylline. Pharmaceutics 2, 275–290.
Sarode, A.L., Sandhu, H., Shah, N., Malick, W., Zia, H., 2013. Hot melt extrusion (HME) for amorphous solid dispersions : Predictive tools for processing and impact of drug-polymer interactions on supersaturation. Eur. J. Pharm. Sci. 48, 371–384.
Seppälä, K., Heinämäki, J., Hatara, J., Seppälä, L., Yliruusi, J., 2010. Development of a New Method to Get a Reliable Powder Flow Characteristics Using Only 1 to 2 g of Powder. AAPS PharmSciTech 11, 402–408.
Shah, S., Maddineni, S., Lu, J., Repka, M.A., 2013. Melt extrusion with poorly soluble drugs. Int. J. Pharm. 453, 233–252.
Sun, C., Grant, D.J.W., 2001. Influence of crystal structure on the tableting properties of sulfamerazine polymorphs. Pharm. Res. 18, 274–280.
Sun, C.C., 2011. Decoding Powder Tabletability: Roles of Particle Adhesion and Plasticity. J. Adhes. Sci. Technol. 25, 483–499. doi:10.1163/016942410X525678
Tarlier, N., Soulairol, I., Bataille, B., Baylac, G., Ravel, P., Nofrerias, I., Lefèvre, P., Sharkawi, T., 2015. Compaction behavior and deformation mechanism of directly compressible textured mannitol in a rotary tablet press simulator. Int. J. Pharm. 495, 410–419.
Treffer, D., Wahl, P., Markl, D., Koscher, G., Roblegg, E., Khinast, J.G., 2013. Hot Melt Extrusion as a Continuous Pharmaceutical Manufacturing Process, in: Melt Extrusion: Materials, Technology and Drug Product Design. Springer, pp. 363–396.
Vachon, M.G., Chulia, D., 1999. The use of energy indices in estimating powder compaction functionality of mixtures in pharmaceutical tableting. Int. J. Pharm. 177, 183–200.
Van Den Mooter, G., 2012. The use of amorphous solid dispersions : A formulation strategy to overcome poor solubility and dissolution rate. Drug Discov. Today Technol. 9, 79–85.
Verstraete, G., Renterghem, J. Van, Bockstal, P.J. Van, Kasmi, S., De Geest, B., De Beer, T., Remon, J.P., Vervaet, C., 2016. Hydrophilic thermoplastic polyurethanes for the manufacturing of highly dosed oral sustained release matrices via hot melt extrusion and injection molding. Int. J. Pharm. 506, 214–221.

Vo, C.L., Park, C., Lee, B., 2013. Current trends and future perspectives of solid dispersions containing poorly water-soluble drugs. Eur. J. Pharm. Biopharm. 85, 799–813.
Warren, D.B., Bergström, C.A.S., Benameur, H., Porter, C.J.H., Pouton, C.W., 2013. Evaluation of the structural determinants of polymeric precipitation inhibitors using solvent shift methods and principle component analysis. Mol. Pharm. 10, 2823–2848.
Yang, Q.W., Flament, M.P., Siepmann, F., Busignies, V., Leclerc, B., Herry, C., Tchoreloff, P., Siepmann, J., 2010. European Journal of Pharmaceutics and Biopharmaceutics Curing of aqueous polymeric film coatings : Importance of the coating level and type of plasticizer. Eur. J. Pharm. Biopharm. 74, 362–370.

Fig. 1. Example of a force-displacement profile recorded in-line on the rotary tablet press defining the different phases during compression.

Fig. 2. Overlay of the temperature sweep experiments on Soluplus (SOL), Kollidon VA 64 (VA 64) and Eudragit EPO (EPO) and their physical mixtures with CEL (35%). Complex viscosity (η^*) is plotted against temperature and the predicted extrudable range is shown (•••).

Fig. 3. XRD-profiles of CEL (a), physical mixtures with 35% CEL for SOL (b), VA 64 (d), EPO (f) and milled extrudates with 35% CEL for SOL (c), VA 64 (e) and EPO (g). The patterns were re-scaled (A.U.) for comparison.

Fig. 4. Example of FT-IR spectra for the neat SOL polymer (···), physical mixture containing 35% CEL (—) and milled extrudates of the formulation with CEL (---) with wavenumbers of the specific peaks.

Fig. 5. Tabletability profiles of the neat polymers (neat), neat polymer hot-melt extrudates (EX) and glassy solutions for formulations containing SOL (left), VA 64 (middle) and EPO (right).

Fig. 6. Compressibility profiles of the neat polymers (neat), neat polymer hot-melt extrudates (EX) and glassy solutions for formulations containing SOL (left), VA 64 (middle) and EPO (right).

Fig. 7. Compactibility profiles of the neat polymers (neat), neat polymer hot-melt extrudates (EX) and glassy solutions for formulations containing SOL (left), VA 64 (middle) and EPO (right).

Fig. 8. Profiles of the plasticity factor in function of compaction pressure for formulations containing SOL (left), VA 64 (middle) and EPO (right), measured in-line at the rotary tablet press.

Fig. 9. Profiles of the measured in-die elastic recovery (IER) normalised by the compaction pressure exerted on the powders, measured in-line at the rotary tablet press for formulations containing SOL (left), VA 64 (middle) and EPO (right).

Fig. 10. Heckel plots for SOL-formulations (left), VA64-formulations (middle) and EPO-formulations (right).

Fig. 11. 'Out-of-die' axial recovery of tablets (n=3) immediately after ejection (full line, —) and after 7 days of storage (point line, ···) for the neat polymers (blue), the milled extrudates (orange**)** and the milled glassy solutions (black) of Soluplus (A), Kollidon VA 64 (B) and Eudragit EPO (C).

Fig. 12. PC_1 vs. PC_2 bi-plot of the determined compaction and flow properties for SOL formulations (blue), VA 64 formulations (green) and EPO formulations (orange) for which the neat polymer (neat, circles), extrudates of the neat polymer (EX, squares) and glassy solutions containing 35% CEL (GS, triangles) are represented in function of the loadings (star symbols): plasticity factor (PF) and the anti-correlated 'in-die' elastic recovery (IER) of the formulations on three exerted compaction pressures (65 MPa, 190 MPa and 510 MPa), the Heckel values D_b and P_y, tablet tensile strength at zero porosity (TS_0) and the flow rate of the formulations.

Fig. 1. Example of a force-displacement profile recorded in-line on the rotary tablet press defining the different phases during compression.

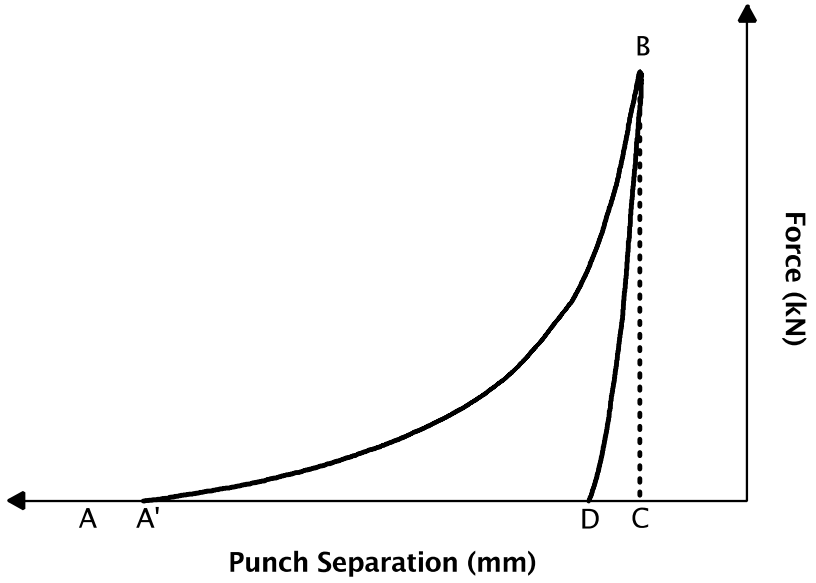

Fig. 2. Overlay of the temperature sweep experiments on Soluplus (SOL), Kollidon VA 64 (VA 64) and Eudragit EPO (EPO) and their physical mixtures with CEL (35%). Complex viscosity (η*) is plotted against temperature and the predicted extrudable range is shown (•••).

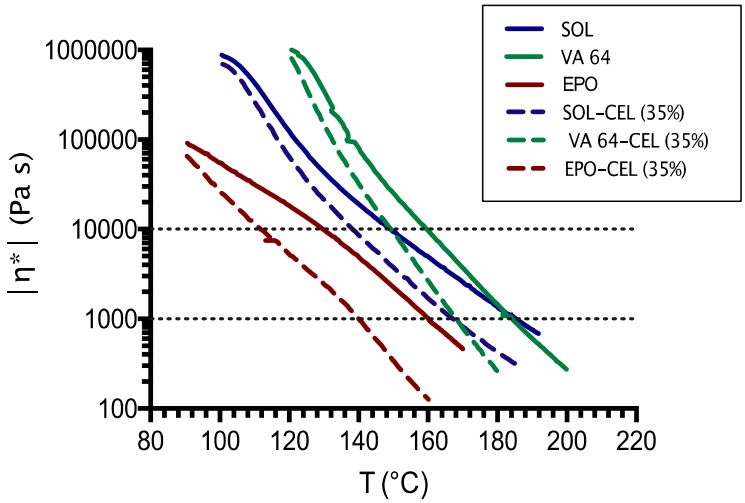

Fig. 3. XRD-profiles of CEL (a), physical mixtures with 35% CEL for SOL (b), VA 64 (d), EPO (f) and milled extrudates with 35% CEL for SOL (c), VA 64 (e) and EPO (g). The patterns were re-scaled (A.U.) for comparison.

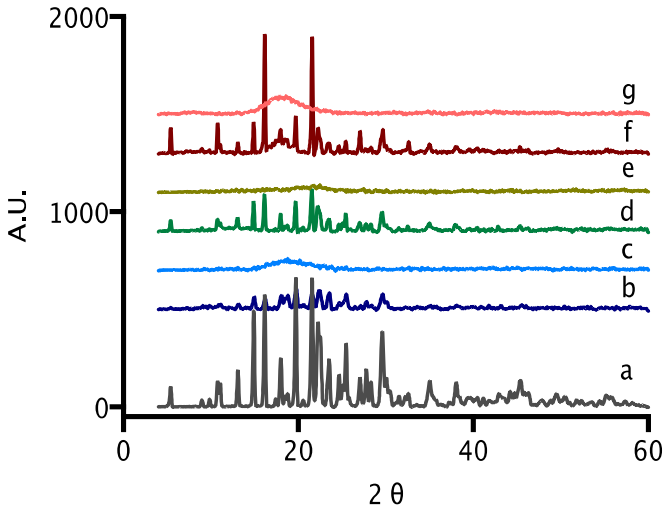

Fig. 4. Example of FT-IR spectra for the neat SOL polymer (···), physical mixture containing 35% CEL (—) and milled extrudates of the formulation with CEL (---) with wavenumbers of the specific peaks.

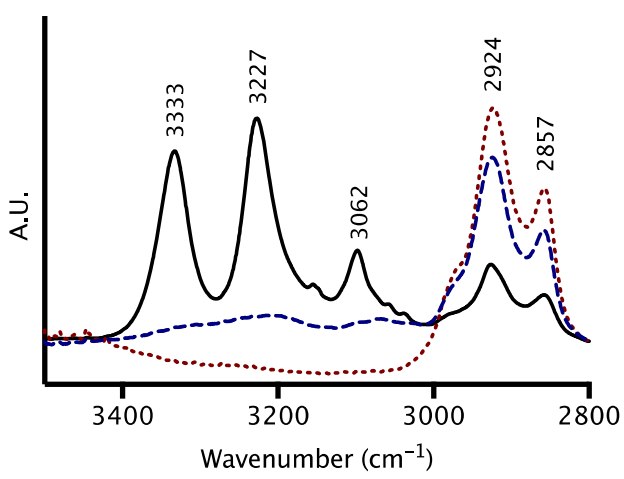

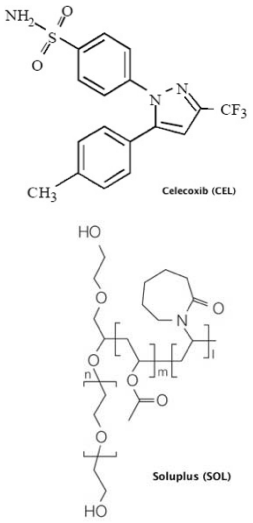

Fig. 5. Tabletability profiles of the neat polymers (neat), neat polymer hot-melt extrudates (EX) and glassy solutions for formulations containing SOL (left), VA 64 (middle) and EPO (right).

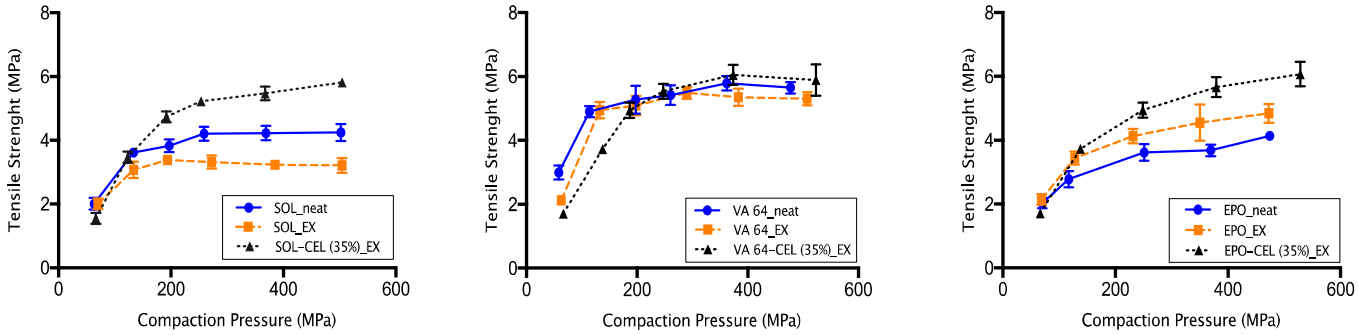

Fig. 6. Compressibility profiles of the neat polymers (neat), neat polymer hot-melt extrudates (EX) and glassy solutions for formulations containing SOL (left), VA 64 (middle) and EPO (right).

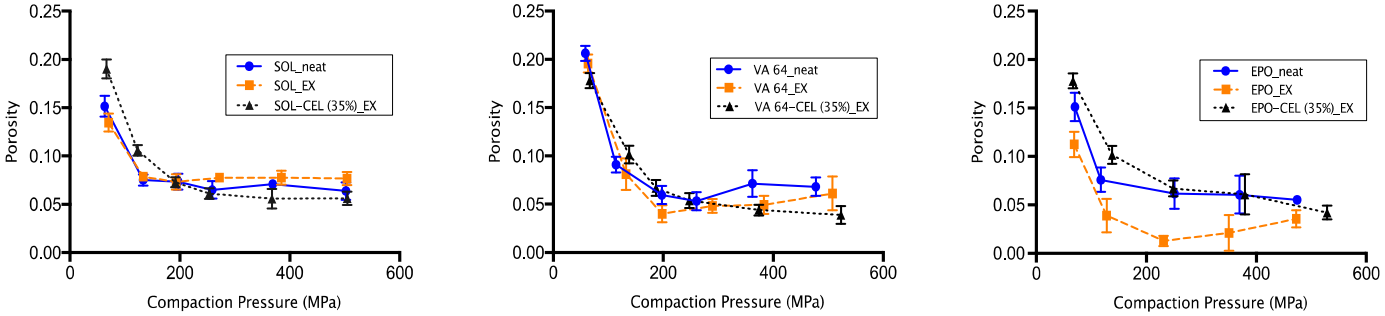

Fig. 7. Compactibility profiles of the neat polymers (neat), neat polymer hot-melt extrudates (EX) and glassy solutions for formulations containing SOL (left), VA 64 (middle) and EPO (right).

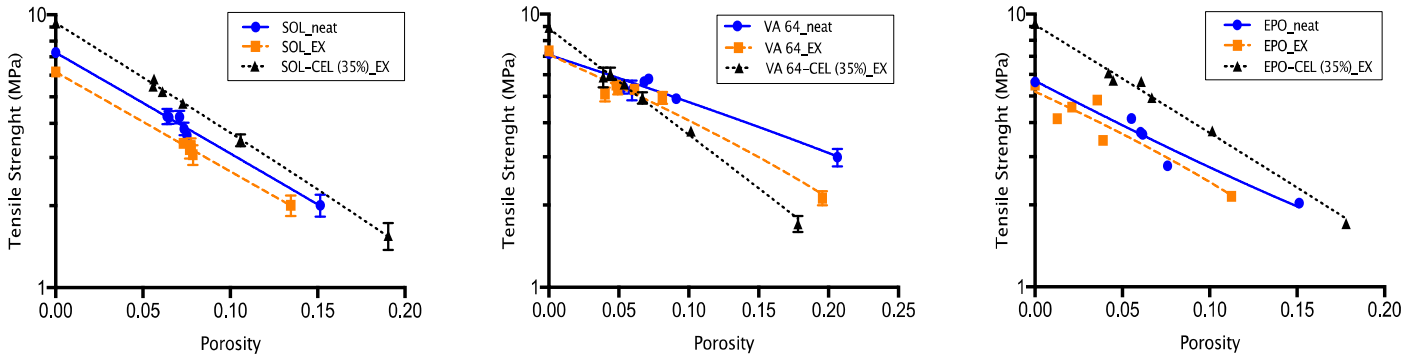

Fig. 8. Profiles of the plasticity factor in function of compaction pressure for formulations containing SOL (left), VA 64 (middle) and EPO (right), measured in-line at the rotary tablet press.

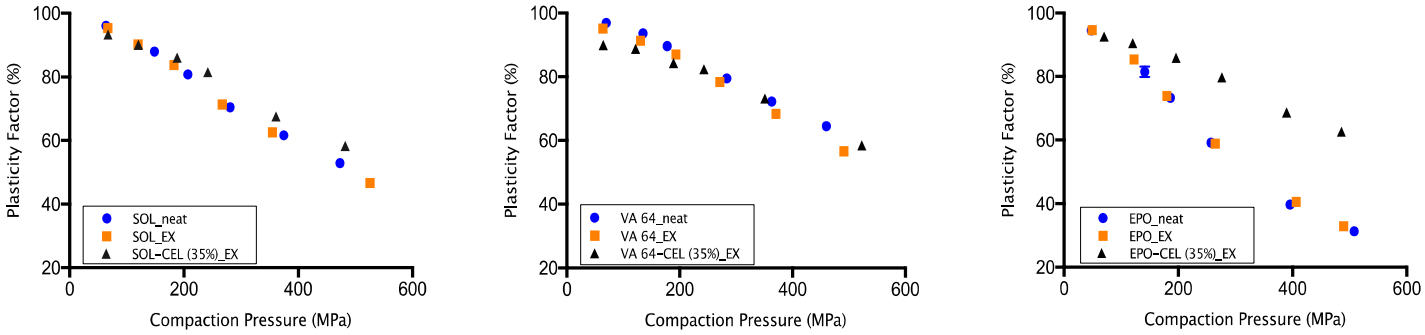

Fig. 9. Profiles of the measured in-die elastic recovery (IER) normalised by the compaction pressure exerted on the powders, measured in-line at the rotary tablet press for formulations containing SOL (left), VA 64 (middle) and EPO (right).

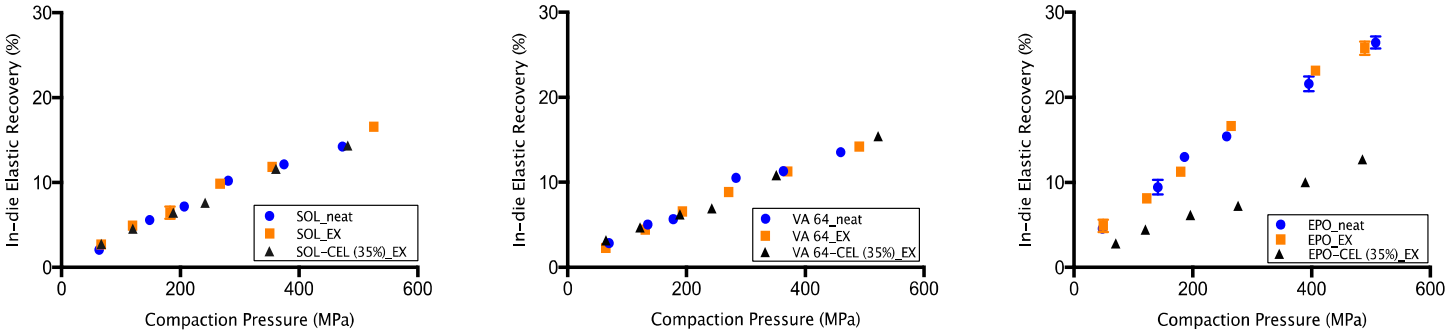

Fig. 10. Heckel plots for SOL-formulations (left), VA64-formulations (middle) and EPO-formulations (right).

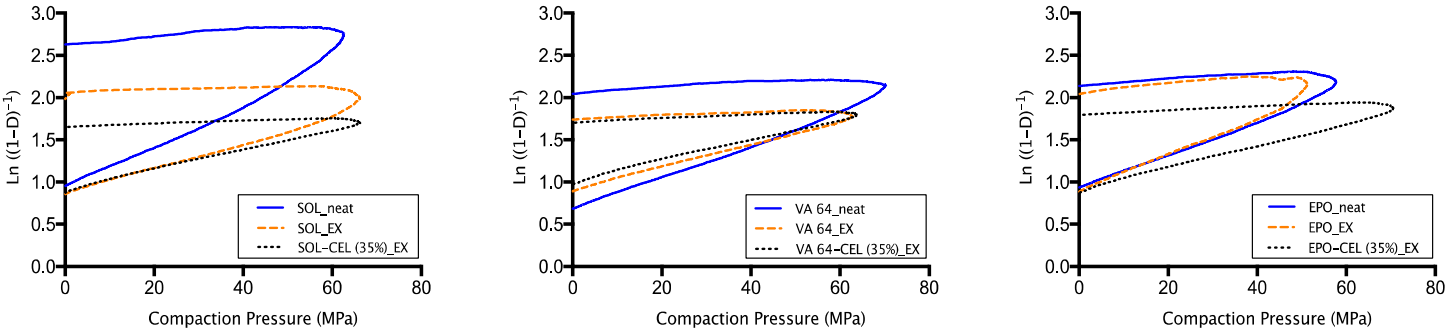

Fig. 11. 'Out-of-die' axial recovery of tablets (n=3) immediately after ejection (full line, —) and after 7 days of storage (point line, ···) for the neat polymers (blue), the milled extrudates (orange**)** and the milled glassy solutions (black) of Soluplus (A), Kollidon VA 64 (B) and Eudragit EPO (C).

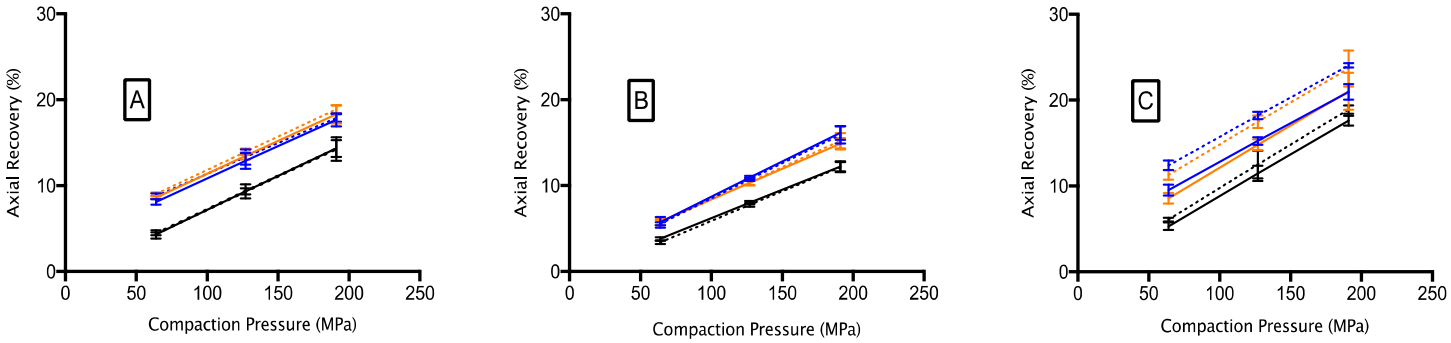

Fig. 12. PC_1 vs. PC_2 bi-plot of the determined compaction and flow properties for SOL formulations (blue), VA 64 formulations (green) and EPO formulations (orange) for which the neat polymer (neat, circles), extrudates of the neat polymer (EX, squares) and glassy solutions containing 35% CEL (GS, triangles) are represented in function of the loadings (star symbols): plasticity factor (PF) and the anti-correlated 'in-die' elastic recovery (IER) of the formulations on three exerted compaction pressures (65 MPa, 190 MPa and 510 MPa), the Heckel values D_b and P_y, tablet tensile strength at zero porosity (TS_0) and the flow rate of the formulations.

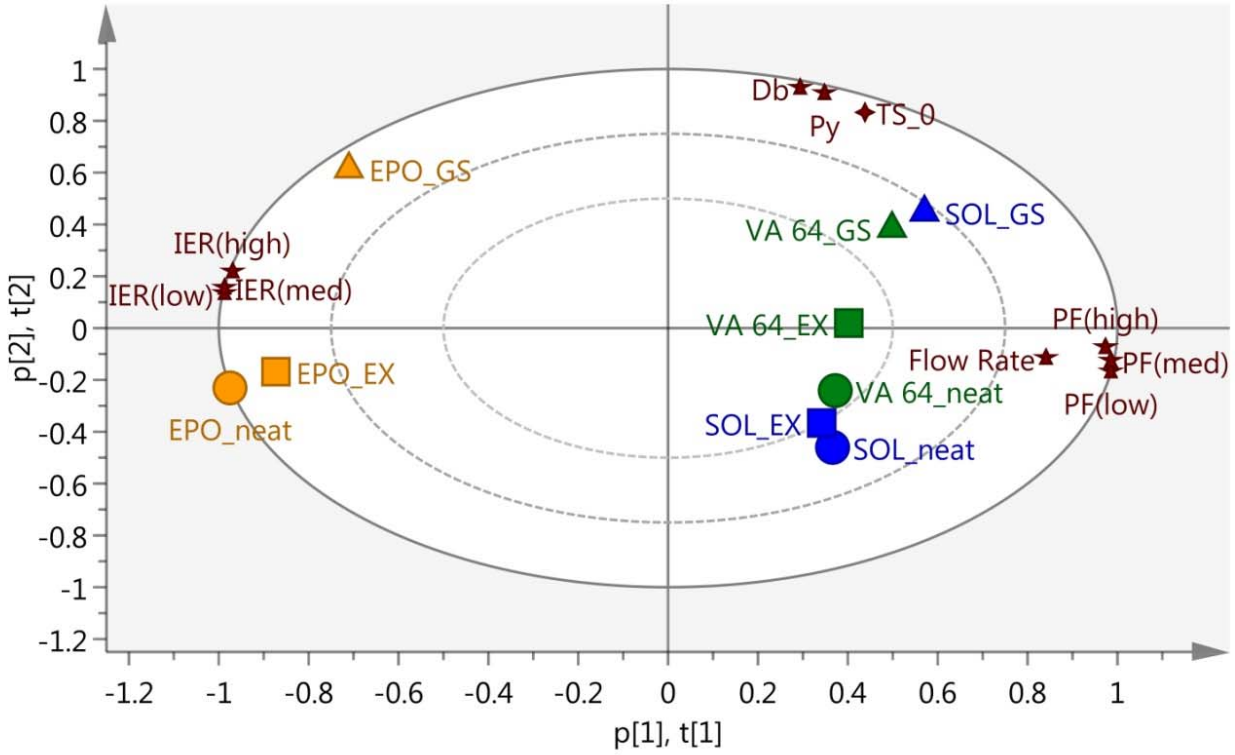

Table 1. Overview of the material characterization data. Degradation temperatures (T_{deg}), glass transition temperatures (T_g), melting points (T_m), extrudable temperature ranges based on complex viscosities ($T_{range\ 10000\text{-}1000\ Pa\ S}$) and barrel extrusion temperatures (T_{ex}).

Table 2. Overview of thermal properties (T_g & T_m) for all polymers non-processed (neat) or as physical mixture with CEL (PM), as extrudates (EX) and extrudates after milling (milled EX).

Table 3. Overview of the physical properties and powder characteristics for all formulations (values are expressed as mean ± st. deviation).

Table 4. Overview of the Heckel parameters (slope k and material constant A) and the derived in-die compaction properties (Heckel mean value P_y and fragmentation factor D_b).

Table 1. Overview of the material characterization data. Degradation temperatures (T_{deg}), glass transition temperatures (T_g), melting points (T_m), extrudable temperature ranges based on complex viscosities ($T_{range\ 10000\text{-}1000\ Pa\ S}$) and barrel extrusion temperatures (T_{ex}).

Formulation	T_{deg} (°C)	T_g (°C)	T_m (°C)	$T_{range\ 10000\text{-}1000\ Pa\ S}$ (°C)	T_{ex} (°C)
CEL	242.2	58.5 ± 0.85	162.9 ± 0.89	-	-
SOL	289.2	64.2 ± 0.89	-	149 - 185	160
SOL-CEL (35%)	-	66.6 ± 1.95	144.2 ± 0.83	138 - 167	140
VA 64	288.9	107.9 ± 0.71	-	160 - 184	170
VA 64-CEL (35%)	-	106.6 ± 3.55	145.4 ± 0.06	149 - 168	150
EPO	250.5	52.5 ± 1.07	-	130 - 160	140
EPO-CEL (35%)	-	52.8 ± 0.39	151.0 ± 3.71	112 - 140	120

Table 2. Overview of thermal properties (T_g & T_m) for all polymers non-processed (neat) or as physical mixture with CEL (PM), as extrudates (EX) and extrudates after milling (milled EX).

Formulation		T_g (°C)	T_m (°C)
SOL	Neat	64.2 ± 0.89[a]	-
	EX	56.9 ± 1.21[b]	-
	Milled EX	56.8 ± 1.82[b]	-
SOL-CEL (35%)	PM	66.6 ± 1.95	144.2 ± 0.83
	Milled EX	52.7 ± 1.15	-
VA 64	Neat	107.9 ± 0.71[a]	-
	EX	106.6 ± 1.21[a]	-
	Milled EX	108.7 ± 1.15[a]	-
VA 64-CEL (35%)	PM	106.6 ± 3.55	145.4 ± 0.06
	Milled EX	103.0 ± 1.16	-
EPO	Neat	52.5 ± 1.07[a]	-
	EX	46.9 ± 1.74[b]	-
	Milled EX	45.7 ± 2.15[b]	-
EPO-CEL (35%)	PM	52.8 ± 0.39	151.0 ± 3.71
	Milled EX	51.5 ± 2.47	-

Means of T_g(^{a,b}) with other superscript are different at the 0.05 level of significance (Tukey) (n=3).
Means of (-) for T_m is the lack of a melting point

Table 3. Overview of the physical properties and powder characteristics for all formulations (values are expressed as mean ± st. deviation).

Formulation		True density (g/cm^3)	Moisture (%)	Mean PSD d_{10} (μm)	d_{50} (μm)	d_{90} (μm)	Specific surface area (m^2/g)	Flow rate (mg/s)
SOL	Neat	1.163 ± 0.009	2.10 ± 0.15	36.0 ± 0.5	81.4 ± 0.9	146 ± 1.2	0.172 ± 0.001	182 ± 12.0
	Milled EX	1.164 ± 0.001	2.10 ± 0.05	35.7 ± 1.5	81.5 ± 1.8	142 ± 2.6	0.161 ± 0.001	165 ± 4.38
SOL-CEL (35%)	Milled EX	1.248 ± 0.000	-	10.6 ± 1.7	57.0 ± 6.6	123 ± 3.0	0.166 ± 0.002	139 ± 10.7
VA 64	Neat	1.213 ± 0.001	3.98 ± 0.01	18.1 ± 0.9	48.2 ± 0.3	82.6 ± 0.5	0.229 ± 0.001	46.7 ± 3.31
	Milled EX	1.211 ± 0.000	4.00 ± 0.06	19.8 ± 0.9	53.2 ± 0.5	94.7 ± 0.8	0.333 ± 0.003	56.9 ± 5.75
VA 64-CEL (35%)	Milled EX	1.262 ± 0.000	-	4.34 ± 0.6	30.0 ± 4.6	104 ± 2.9	0.382 ± 0.002	61.2 ± 2.12
EPO	Neat	1.108 ± 0.003	0.99 ± 0.03	4.82 ± 0.1	8.85 ± 0.4	18.8 ± 4.0	1.274 ± 0.004	7.90 ± 0.39
	Milled EX	1.085 ± 0.004	1.02 ± 0.01	3.40 ± 0.7	8.44 ± 1.1	49.1 ± 7.0	2.507 ± 0.008	7.70 ± 1.67
EPO-CEL (35%)	Milled EX	1.215 ± 0.003	-	7.22 ± 0.7	14.9 ± 0.7	64.8 ± 3.8	0.562 ± 0.006	15.2 ± 1.67

Table 4. Overview of the Heckel parameters (slope k and material constant A) and the derived in-die compaction properties (Heckel mean value P_y and fragmentation factor D_b).

Formulation		k (1/MPa)	P_y (MPa)	A	D_b
SOL	Neat	0.022	45.42 ± 1.43	0.952	0.0047
	Milled EX	0.017	58.59 ± 3.67	0.915	0.0122
SOL-CEL (35%)	Milled EX	0.011	96.66 ± 1.31	0.957	0.0348
VA 64	Neat	0.017	57.50 ± 0.97	0.726	0.0151
	Milled EX	0.012	80.02 ± 1.49	0.940	0.0226
VA 64-CEL (35%)	Milled EX	0.011	92.49 ± 1.17	1.072	0.0331
EPO	Neat	0.018	55.01 ± 2.24	0.930	0.0037
	Milled EX	0.020	49.33 ± 0.76	0.915	0.0150
EPO-CEL (35%)	Milled EX	0.012	84.68 ± 1.20	0.952	0.0312